

# Controlled disorder - induced peak effect in single crystalline $\text{Ca}_3\text{Rh}_4\text{Sn}_{13}$ superconductor

Sunil Ghimire,<sup>1, 2</sup> Kamal R. Joshi,<sup>1, 2</sup> Elizabeth H. Krenkel,<sup>1, 2</sup> Marcin Kończykowski,<sup>3</sup> Romain Grasset,<sup>3</sup> Makariy A. Tanatar,<sup>1, 2</sup> Shuzhang Chen,<sup>4, 5</sup> Cedomir Petrovic,<sup>4, 5, 6, 7</sup> and Ruslan Prozorov<sup>1, 2, \*</sup>

<sup>1</sup>Ames National Laboratory, Ames, Iowa 50011, USA

<sup>2</sup>Department of Physics & Astronomy, Iowa State University, Ames, Iowa 50011, USA

<sup>3</sup>Laboratoire des Solides Irradiés, CEA/DRF/IRAMIS, École Polytechnique,

CNRS, Institut Polytechnique de Paris, F-91128 Palaiseau, France

<sup>4</sup>Condensed Matter Physics and Materials Science Department,  
Brookhaven National Laboratory, Upton, New York 11973, USA

<sup>5</sup>Department of Physics and Astronomy, Stony Brook University, Stony Brook, New York 11794-3800, USA

<sup>6</sup>Shanghai Key Laboratory of Material Frontiers Research in Extreme Environments (MFree),  
Shanghai Advanced Research in Physical Sciences (SHARPS), Pudong, Shanghai 201203, China

<sup>7</sup>Department of Nuclear and Plasma Physics, Vinca Institute of  
Nuclear Sciences, University of Belgrade, Belgrade 11001, Serbia

(Dated: 10 September 2024)

The effects of 2.5 MeV electron irradiation on the magnetic properties of single crystals of the Remeika series superconductor  $\text{Ca}_3\text{Rh}_4\text{Sn}_{13}$  were studied using high-frequency AC susceptometry, magnetization, and electrical transport. This low-pinning cubic stannide is an ideal system to examine the effects of a controlled non-magnetic point-like disorder. The measured Campbell penetration depth was used to extract the magnetic field dependence of the unrelaxed critical current density,  $j_c(H)$ . The critical current is a monotonic function of a magnetic field in pristine state. However, even the lowest dose of electron irradiation causes a pronounced peak effect in  $j_c(H)$ . The peak effect is also observed in magnetization measurements performed with different characteristic time windows. We conclude that additional defects trigger the appearance of a disordered vortex phase at magnetic fields close to the upper critical field, and the peak effect is the result of a crossover from the weakly distorted low-field vortex lattice to the disordered high-field vortex phase. These results strongly support the static picture of the peak effect formation in  $\text{Ca}_3\text{Rh}_4\text{Sn}_{13}$  in which this is a feature of the critical current density,  $j_c(H)$ , and not the result of magnetic field-dependent vortex relaxation,  $j(H, t)$ .

## I. INTRODUCTION

Understanding the physics of Abrikosov vortices [1] is crucially important for potential applications of superconductors [2–5]. The vortex lattice is a unique, highly tunable quantum system that exhibits a plethora of fascinating properties and effects, which are of great interest from a fundamental point of view [2, 3, 6–9]. One prominent feature is the non-monotonic behavior of magnetization as a function of an applied magnetic field and, sometimes as a function of temperature, known as the “peak effect” or “second magnetization peak” [10–24]. In some high- $T_c$  cuprate superconductors, this effect is so pronounced and unusual that it was often called a “fishtail” to distinguish it from the “peak effect” of conventional superconductors [2, 3, 25–27]. Currently, these terms are often used interchangeably [16, 26, 28–34].

The explanation of the non-monotonic behavior can be divided into two categories, static and dynamic. In the former, the actual critical current density,  $j_c(H)$ , is a non-monotonic function of a magnetic field, whereas the latter explanation is based on the idea that vortex relaxation is faster at lower magnetic fields and, therefore,

the measured current density (or magnetization) becomes non-monotonic. Elucidation of the nature of the peak effect is important because a static picture would require the appearance of novel high-field vortex phases and pinning mechanisms. Every measurement technique has a finite time window [8, 35]. For example, in a ubiquitous *Quantum Design* magnetic property measurement system (MPMS), each data point is collected over several seconds. In commonly used amplitude-domain AC susceptibility, the frequencies range from 1 to 10 kHz [35]. Magnetic relaxation is exponentially fast at  $j \rightarrow j_c$ , so the measured persistent current density may become non-monotonic even if the critical current is monotonic. In fact, this scenario is predicted by the theory of collective pinning and creep [2].

Among the static mechanisms suggested for the peak effect is the earliest model of vortex lattice softening approaching  $H_{c2}$  [11]. After the discovery of “fishtail” in many cuprate superconductors, various models were suggested. For example, different low- and high-field pinning mechanisms [25], order-disorder (weak to strong pinning) transition [21, 23, 36], perhaps accompanied by a crossover from collective to plastic creep regimes [32, 37], as well as competing different vortex phases [38]. Finally, there were suggestions that the irreversible peak effect may be a possible signature of the inhomogeneous

\* Corresponding author: prozorov@ameslab.gov

Fulde–Ferrell–Larkin–Ovchinnikov (FFLO) state [39–43]. For example, the FFLO state was proposed for some heavy fermion compounds, such as  $\text{CeRu}_2$ ,  $\text{UPd}_2\text{Al}_3$  [44, 45]. The later relation between the peak effect [46] and the field-induced state was not supported by the thermal conductivity and heat capacity measurements in  $\text{Sr}_2\text{RuO}_4$  [47, 48].

Since the origin of magnetic irreversibility in superconductors is in the vortex pinning, it is natural to study the peak effect phenomenon by controlling the type and concentration of defects. In general, controlled disorder has been used as a powerful tool to study fundamental properties of superconductors, such as the superconducting gap structure and possible topological behavior. These works form a large body of literature, and here we can only mention a few representative works [49–60]. In the remainder of the paper, we focus on vortex-related properties.

There are several ways to introduce controlled disorder, for example, chemical substitution (doping) [24, 29, 61–63], but it has the disadvantage of changing the Fermi level and/or exerting internal “chemical pressure”, thus altering the basic properties of a studied superconductor. Another method of introducing disorder, free from these side effects, is irradiation with different energetic particles. Some commonly used types include heavy ions, which often produce columnar defects that match tubular vortex geometry [38, 64–73], protons that produce point-like disorder and/or extended clusters [51, 54, 56, 57, 60, 74–77], and electrons that create point-like disorder of vacancies and interstitials [38, 55, 78–82]. Other projectiles, such as neutrons [12, 53, 61, 62, 68, 83–87],  $\gamma$ -rays [88],  $\alpha$ -particles [50, 89], are also used, but it is more difficult to determine the nature of the induced defects.

The effect of irradiation specifically on the peak effect has been reported for electron irradiation [80, 81], proton irradiation [75, 76], neutron irradiation [12, 62], and heavy-ion irradiation [64, 67, 73].

To investigate the effect of disorder, it is important to start with a low-pinning superconductor. In recent years, we have studied the structure of the superconducting energy gap and the coexistence of the charge density wave (CDW) and superconductivity in some members of the stannide family,  $(\text{Ca},\text{Sr})_3(\text{Ir},\text{Rh})_4\text{Sn}_{13}$  [90, 91], which belongs to a large family of compounds known as the 3-4-13 Remeika series [92, 93]. For fractional compositions, there is a structural quantum critical point (QCP) underneath the “dome” of superconductivity on the  $T_c(x)$  phase diagram [91, 94, 95]. Here we study the end member,  $\text{Ca}_3\text{Rh}_4\text{Sn}_{13}$ , which does not have CDW order. This compound and  $\text{Ca}_3\text{Ir}_4\text{Sn}_{13}$  (which has CDW ordering) are often studied together and both show very low pinning and a pronounced peak effect in AC and DC field measurements [14, 15, 17, 18, 20, 96]. Therefore, they are very attractive systems for investigating the effect of artificially controlled disorder. Non-monotonic AC susceptibility has been reported in other 3-4-13 compounds,

for example  $\text{Y}_3\text{Ru}_4\text{Ge}_{13}$  and  $\text{Lu}_3\text{Os}_4\text{Ge}_{13}$  [19]. Previous studies of the peak effect in  $\text{Ca}_3\text{Rh}_4\text{Sn}_{13}$  using DC and low-frequency AC susceptibility (113 Hz, 2 Oe AC field amplitude) proposed a change from weak to strong pinning as an explanation [14].

We note that another 3-4-13 stannide,  $\text{Yb}_3\text{Rh}_4\text{Sn}_{13}$ , has vortex phase diagram similar to  $\text{Ca}_3\text{Rh}_4\text{Sn}_{13}$ . It exhibits an irreversible peak effect in resistivity and magnetization. It was suggested that this could be an FFLO state, but the analysis showed that this is not the case [97, 98]. Although the existence of the peak effect in 3-4-13 compounds is firmly established, the question of whether it has a dynamic or static origin remains open.

To the best of our knowledge, there have been no studies of the effect of irradiation-induced disorder on the vortex properties of these superconductors. This contribution is intended to fill this gap. We disentangle the dynamic (flux creep) and static (actual non-monotonicity of  $j_c(H)$ ) by measuring both conventional magnetization that reveals the relaxed state and the Campbell penetration depth, which contains the true unrelaxed  $j_c$  as a parameter. Random point defects are created by 2.5 MeV electron irradiation. Importantly, the same sample was repeatedly measured between irradiation sessions, reaching a substantial cumulative dose of  $4.36 \times 10^{19}$  electrons/cm<sup>2</sup>. We show that electron irradiation induces non-monotonic  $j_c(H)$ , lending strong support to the static origin of the peak effect.

## II. METHODS AND SAMPLES

**Samples:** Single crystals of stoichiometric  $\text{Ca}_3\text{Rh}_4\text{Sn}_{13}$  were grown using a high temperature self-flux method [99]. The composition was verified by X-ray diffraction measured on a Rigaku Miniflex powder diffractometer. The elemental analysis was performed using energy-dispersive X-ray spectroscopy in a JEOL JSM-6500 scanning electron microscope. The same samples were used in previous studies that provide more details on their characterization [90, 91].

**Electrical resistivity:** Electrical resistivity was measured with bar-shaped single crystals in a standard four-probe configuration. The crystals were etched with HCl, cut with a wire saw, and polished to a typical size of  $(1 - 2) \times 0.2 \times 0.4$  mm<sup>3</sup>. The contacts were formed by soldering 50  $\mu\text{m}$  silver wires with tin-silver solder with a typical contact resistance below 100  $\mu\Omega$  [90, 100]. In the experiment, the sample was first measured, then irradiated at low temperature as described below, removed from the chamber at room temperature, measured again, and the process was repeated, adding more irradiation dose.

**Magnetization:** Magnetization was measured using a *Quantum Design* vibrating sample magnetometer (VSM) option in a physical property measurement system (PPMS). During the measurement, the sample vibrates with a peak amplitude of 2 mm at a frequency of

40 Hz, and the signal is averaged over one second. This device is particularly suitable for high-resolution measurements of irreversible magnetic response because it allows for a continuous sweep of the magnetic field at rates between 12 Oe/s and 200 Oe/s, thus probing directly the effects of vortex creep.

**London and Campbell penetration lengths:** The temperature-dependent variation of the London penetration depth,  $\Delta\lambda(T)$ , and of the Campbell length,  $\lambda_C$ , was measured using a self-oscillating tunnel-diode resonator (TDR) [101–104]. Briefly, the TDR tank circuit is always locked onto its resonant frequency (approximately 14 MHz in our case), producing an AC magnetic field of approximately 20 mOe. With a sample inserted into an inductor, the total inductance depends on the magnetic susceptibility of the sample,  $\chi(T, B)$ . This results in a frequency shift with respect to the empty resonator value,  $f_0$ ,  $\Delta f \equiv f(T, B) - f_0 = -G\chi$ , where  $G$  is the calibration factor described in detail elsewhere [101, 104]. This factor includes the filling factor (the ratio of sample to coil volumes), sample shape (via the demagnetizing factor), and the frequency of the unperturbed (empty) resonator,  $f_0$ . Importantly, in our setup, the constant  $G$  is measured for each sample by mechanically pulling it out of the coil at the base temperature (0.4 K in our  $^3\text{He}$  cryostat). The small-amplitude linear magnetic susceptibility of a superconductor of arbitrary shape is given by  $\chi = \lambda_m/R \tanh(R/\lambda_m) - 1$ , where  $\lambda_m$  is the measured total magnetic penetration depth and  $R$  is the effective dimension calculated from the actual sample dimensions [104]. For typical submillimeter-sized crystals,  $R \sim 100 - 200 \mu\text{m}$ . The sample used in this study had dimensions of  $650 \times 595 \times 185 \mu\text{m}$ , which yields the effective  $R = 103 \mu\text{m}$ . Therefore,  $R \gg \lambda$  for most of the temperature interval ( $\lambda(T)$  only doubles at  $T = 0.95T_c$ ), and we can assume  $\tanh R/\lambda \approx 1$ . Hence,  $\Delta\lambda(T, B) = RG\delta f(T, B)$ , where  $\delta f = \Delta f(T, B) - \Delta f(T_{\min}, B) = f(T, B) - f(T_{\min}, B)$  is measured from the base temperature. The absolute value of  $\lambda_m(T)$  is difficult to measure, but the shift  $\Delta\lambda_m(T)$  is measured with the angström-level precision [101, 105]. When no external DC magnetic field is applied, the measured penetration depth is the London penetration depth. When the external magnetic field is applied, the measured penetration depth is a combination of London and Campbell lengths,  $\lambda_m^2 = \lambda_L^2 + \lambda_C^2$  [3, 106, 107].

In this experiment, we first measure the change in the London penetration depth,  $\Delta\lambda_L(T) = \lambda_m(T, B = 0)$ , and calculate the total using a known absolute value,  $\lambda(0) = 330 \text{ nm}$  in our material [90],  $\lambda_L(T) = \lambda_L(0) + \Delta\lambda_L(T)$ . Since at  $T_c$  the frequency shift is limited by the normal metal skin depth, we use it as the reference point, so that the total depth is  $\lambda_m(T) = \lambda_L(0) + \Delta\lambda_m(T, B)$ . Then, the Campbell length is obtained as  $\lambda_C = \sqrt{\lambda_m^2 - \lambda_L^2}$ .

**Electron irradiation:** Point-like disorder was introduced at the SIRIUS facility in the Laboratoire des Solides Irradiés at École Polytechnique, Palaiseau,

France. Electrons are accelerated in a pelletron-type linear accelerator to 2.5 MeV and knock out ions, creating vacancy-interstitial Frenkel pairs [108, 109]. During irradiation, the sample is held in liquid hydrogen at around 20 K to ensure efficient heat removal and to prevent immediate recombination and clustering of produced defects. The acquired irradiation dose is determined by measuring the total charge collected by a Faraday cage located behind the sample. As such, the acquired dose is measured in “natural” units of  $\text{C}/\text{cm}^2$ , so that  $1 \text{ C}/\text{cm}^2 \equiv 1/e \approx 6.24 \times 10^{18}$  electrons per  $\text{cm}^2$ . For single crystals of  $\text{Ca}_3\text{Rh}_4\text{Sn}_{13}$ , the total cross section to create defects for any ion is 137 barn at 2.5 MeV and using a generic knock-out threshold barrier of 25 eV [90, 108, 109]. Therefore, the maximum concentration of defects is approximately one defect per ten unit cells (a unit cell volume is  $919.3 \text{ \AA}^3$  and contains two formula units, 40 atoms,  $Z = 20$ ) for the initial dose of  $3 \text{ C}/\text{cm}^2$  and per about four unit cells for the maximum dose of  $7 \text{ C}/\text{cm}^2$ . The mean distance between the defects is 2.1 nm for  $3 \text{ C}/\text{cm}^2$  and 1.6 nm for  $7 \text{ C}/\text{cm}^2$ . Upon warming the sample to room temperature, some pairs recombine, and some migrate to various sinks (dislocations, surfaces, etc.). This reduces the number of defects by 30% or so and leaves a metastable population of point defects. The stability of these remaining defects depends on the material, but in general is quite robust. The nature of the defects produced by electron irradiation has been well studied with microscopy and x-ray spectroscopy, as well as with simulations [108–113]. The actual amount of disorder in a specific sample is monitored by measuring the residual resistivity. In most superconductors, the same irradiated sample measured months and years apart showed only a little change. Additional details can be found elsewhere [52, 90].

We note that different samples were used for resistivity and penetration depth measurements, due to different requirements to the sample size and the electrical contacts attached to transport samples. As a result, the resistivity and penetration depth samples received different doses of irradiation. Multiple irradiations with subsequent measurements were performed for each sample and technique between the irradiation sessions.

### III. RESULTS AND DISCUSSION

#### A. Resistivity

Figure 1 shows temperature-dependent resistivity of a single crystal  $\text{Ca}_3\text{Rh}_4\text{Sn}_{13}$  before and after four irradiation runs. The legend shows the cumulative collected dose of electron irradiation:  $0.6 \text{ C}/\text{cm}^2$ ,  $1.2 \text{ C}/\text{cm}^2$ ,  $1.6 \text{ C}/\text{cm}^2$ , and  $2 \text{ C}/\text{cm}^2$ . Lower inset focuses on the superconducting transition. As can be seen,  $\rho(T)$  just above  $T_c$  is practically temperature independent and so we can use its value at  $T_c$  as a proxy for residual resistivity,  $\rho_0 \approx \rho(T_c)$ . The upper inset shows a prac-

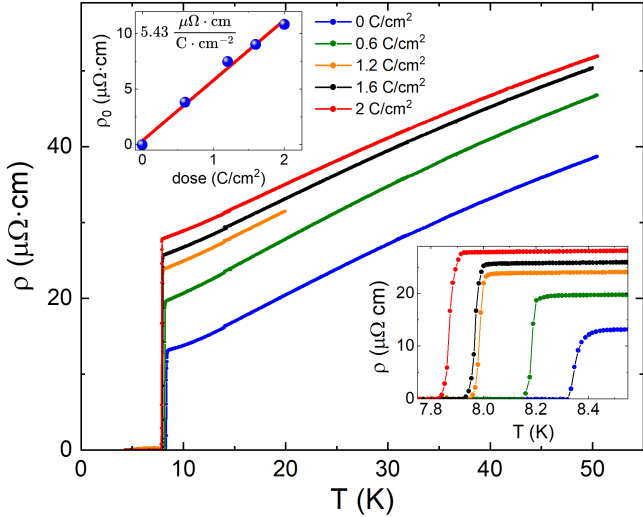


FIG. 1. Temperature-dependent resistivity of  $\text{Ca}_3\text{Rh}_4\text{Sn}_{13}$  single crystal. Blue curve shows pristine sample, green  $0.6 \text{ C}/\text{cm}^2$ , orange  $1.2 \text{ C}/\text{cm}^2$ , black  $1.6 \text{ C}/\text{cm}^2$ , and red  $2 \text{ C}/\text{cm}^2$  stages of electron irradiation. Note that the cumulative dose is shown. The lower inset zooms on the superconducting transition. At the maximum dose, the irradiation suppresses  $T_c$  by 0.5 K and increases residual resistivity,  $\rho_0$ , from 7 to  $18 \mu\Omega \cdot \text{cm}$ . The upper inset shows the change of the residual resistivity as a function of  $T_c$  with the slope of  $d\rho_0/d(\text{dose}) = 5.43 \mu\Omega \cdot \text{cm}/(\text{C}/\text{cm}^2)$ .

tically linear  $\rho_0(\text{dose})$  with the slope of  $d\rho_0/d(\text{dose}) = 5.43 \mu\Omega \cdot \text{cm}/(\text{C}/\text{cm}^2)$ . At the maximum dose of  $2 \text{ C}/\text{cm}^2$ , the irradiation suppresses  $T_c$  by 0.5 K and increases the residual resistivity from 7 to  $18 \mu\Omega \cdot \text{cm}$ .

## B. London penetration depth

The change of the London penetration depth,  $\Delta\lambda_L(T, B = 0) = \lambda_L(T, B = 0) - \lambda_L(T_{\min}, B = 0)$  as a function of temperature is shown in Fig. 2. The low-temperature behavior is exponentially attenuated, which is consistent with a fully gapped Fermi surface [90]. Therefore, we can safely assume that  $\lambda(T_{\min}, B = 0) \approx \lambda(T = 0, B = 0)$ . The onset transition temperature in the pristine state is  $T_{c0} = 8.04 \text{ K}$ . The same sample was electron irradiated multiple times accumulating doses of  $3 \text{ C}/\text{cm}^2$ ,  $5 \text{ C}/\text{cm}^2$ , and  $7 \text{ C}/\text{cm}^2$  with  $T_c$  listed next to each curve in Fig. 2. The inset in Fig. 2 shows  $T_c$  plotted against dose (bottom axis) and residual resistivity (top axis). The resistivity values for sample 2 were obtained from the  $\rho_0$  (dose) dependence established in Fig. 1. The transition temperature decreases, uniformly dropping to  $T_c = 6.96 \text{ K}$  at the maximum dose of  $7 \text{ C}/\text{cm}^2$ . Importantly, the superconducting transition remains very sharp, which means that the defects created by irradiation are homogeneously distributed throughout the sample. At  $T_c$ , the penetration depth does not diverge but is cut off by the normal metal skin depth,  $\sim \sqrt{\rho(T_c)}$ .

Therefore, its value increases with the dose providing independent evidence that the resistivity increases with electron irradiation.

## C. Campbell penetration depth: theoretical summary

The Campbell penetration depth is the characteristic length at which the small-amplitude AC field,  $H_{AC}$ , propagates into the superconductor in the presence of vortices,  $H(r) = H_{DC} + H_{AC}e^{-r/\lambda_C}$ , where  $H_{DC}$  is the applied DC magnetic field [114, 115]. Note that in this section, we explicitly use the SI units and label the internal position-dependent magnetic induction  $B(r)$ , and the applied magnetic field strength is labeled  $H$ . Importantly, it is assumed that vortices are not driven out of their potential wells,  $U(r)$ . Quite generally, Campbell length is given by the curvature of the pinning potential, called the Labusch parameter,  $\alpha = d^2U(r)/dr^2$  [3, 6, 102, 106, 107, 114, 115],

$$\lambda_C^2 = \frac{\phi_0 B_0}{\mu_0 \alpha(r_B)} \quad (1)$$

where  $r_B$  is the “vortex bias” position from the potential well’s center. Vortices are biased by the Lorentz force exerted by the macroscopic persistent (Bean) current density [6, 116, 117] due to the vortex density gradient,  $\mu_0 \mathbf{j} = \nabla \times \mathbf{B}(\mathbf{r})$ . This force is balanced by the pinning force at  $r = r_B$  [6]. True critical current is achieved at a maximum force corresponding to some displacement,  $r_p$ , called the “radius” of the pinning potential and depends on the shape of the potential well,  $U(r)$ . The Labusch parameter can be evaluated using Eq. 1,  $\alpha = \phi_0 B_0 / \mu_0 \lambda_C^2$ . In the original Campbell model, the potential is parabolic,  $U(r) = \frac{1}{2}\alpha_L r^2$  for  $r \leq r_p$  and is zero otherwise. The Labusch parameter,  $\alpha(r) = \alpha_L$  is now the Labusch constant [6]. In this case, there is no maximum of the force,  $f(r) = -dU/dr = -\alpha_L r$ , and an artificial cutoff of the pinning potential at the pinning potential range,  $r_p$ , was introduced. It is usually assumed to be equal to the coherence length, but of course can be larger, for example in the collective pinning theory [2]. Realistic pinning potentials must satisfy,  $\lim_{r \rightarrow \infty} (U(r)) = 0$ , so there is always a maximum, which sets the natural scale for  $r_p$ . It is important to note that, by definition, when the restoring force,  $dU/dr$ , is maximal (and this defines the critical current density,  $j_c$ ), the Labusch parameter,  $\alpha = d^2U(r_p)/dr^2 = 0$ . Then it follows from Eq. 1 that the Campbell length diverges at  $j = j_c$ . This was missing in the original model.

To probe the shape of the pinning potential, three different measurement protocols were employed. In zero-field cooling (ZFC), a sample is cooled to a target temperature below  $T_c$  without an external magnetic field, then a specified dc magnetic field is applied and measurements are performed on warming. In a field-cooled

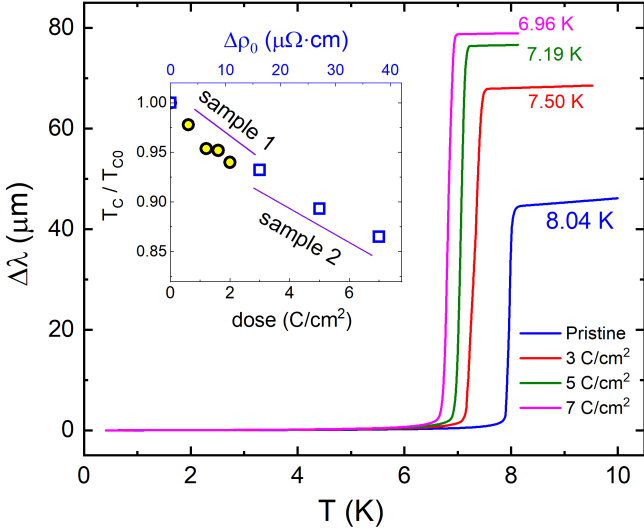


FIG. 2. Temperature variation of the London penetration depth,  $\Delta\lambda_L(T)$ . The blue curve shows the pristine sample, and red, green, and magenta show  $\Delta\lambda_L(T)$  after irradiation with 3, 5, and 7  $\text{C}/\text{cm}^2$ , respectively. The onset of the superconducting transition temperature is listed next to each curve. Inset shows the rate of  $T_c$  suppression with the increasing dose of irradiation (bottom axis) and the change of residual resistivity with respect to the pristine state (top axis). Sample 1 is the resistivity-measurements sample of Fig. 1, and sample 2 is the penetration depth sample that acquired larger doses of irradiation.

(FC) protocol, the data are taken on cooling from above  $T_c$  in a fixed dc magnetic field (FCC) or on warming after cooling from above  $T_c$  in a fixed magnetic field (FCW). Usually, this sequence is performed: ZFC  $\rightarrow$  FCC  $\rightarrow$  FCW to explore any possible hysteretic behavior.

Application of the external magnetic field at low temperature in a ZFC protocol results in an inhomogeneous gradient vortex density distribution with macroscopic persistent current density described by the Bean model [116, 117]. By definition, at the critical current density,  $j_c$ , the barrier to vortex creep is zero, so there is always some relaxation, determined by the time window of the experiment [2]. The initial relaxation is exponentially fast. Note that despite the fact that we use a 14 MHz oscillator, the vortex position inside the pinning potential is still determined by the Bean persistent current, and tiny oscillations of vortices only probe the local curvature. In FC measurements, there is no vortex gradient, no persistent current, and vortices are located at the bottom of their potential wells. Therefore, a comparison of the ZFC and FC measurements allows us to draw conclusions about the shape of  $U(r)$ , albeit through its second derivative. In the case of a parabolic potential, there is no difference between the ZFC and the FC curves, since the curvature is constant and is independent of the Bean current. Measurements of different superconductors show a variety of behaviors, from completely reversible to significantly hysteretic [102, 118–120].

Most importantly, measurements of Campbell length provide access to the critical current density. In a field-cooled protocol, the vortex density distribution is uniform, in which case vortices oscillate near the bottom of the pinning potential. Regardless of its overall shape, near the center  $U(r)$  can always be approximated by the parabola. For example, a realistic pinning potential is  $U(r) = \frac{1}{2}U_0 \tanh(x^2)$ , where  $x = r/r_p$  and the maximum restoring force is achieved at  $x_c = 0.72$ . Without biasing current, near  $r = 0$ , this potential is parabolic,  $U(r) = \frac{1}{2}U_0(r/r_p)^2$ , which is just the original Campbell model but contains the value of  $r_p$  obtained from the full model. The critical current is

$$j_c = \gamma_c \frac{U_0}{\phi_0 r_p} = \gamma_c \frac{r_p \alpha_L}{\phi_0} = \gamma_c \frac{r_p B_0}{\mu_0 \lambda_C^2} \quad (2)$$

where  $\alpha_L = \alpha(r = 0)$  and dimensionless parameter  $\gamma_c$  depends on the shape of the potential,  $\gamma_c = dU/dx|_{x=x_c}$ . For the potential considered here,  $\gamma_c = 0.56$ . Therefore, even without knowing  $\gamma_c$ , we can estimate the true critical current density,  $j_c$ , from the FC measurements of the Campbell penetration depth up to a coefficient of the order of unity. For convenience of calculations, in practical units, Eq. 2 is:

$$j_c \left[ \frac{\text{A}}{\text{cm}^2} \right] = \gamma_c 7.9577 \times 10^{10} \frac{B_0 [\text{T}] r_p [\text{nm}]}{(\lambda_C [\text{nm}])^2} \quad (3)$$

#### D. Campbell penetration depth: experimental results

Figure 3, shows the Campbell penetration depth,  $\lambda_C = \sqrt{\lambda_m^2 - \lambda_L^2}$ , for a pristine sample (a), and that same sample after electron irradiation with doses of (b) 3  $\text{C}/\text{cm}^2$ , (c) 5  $\text{C}/\text{cm}^2$ , and (d) 7  $\text{C}/\text{cm}^2$ . The solid lines correspond to ZFC measurements. The dashed lines show the FC measurements. Note that vertical and horizontal scales are the same for each graph in Fig. 3 to facilitate comparison and visualize the effect of irradiation. The higher cut-off values of  $\lambda_C \rightarrow T_c(H)$  correspond to the normal-state skin depth that increases because normal state resistivity increases after irradiation. Importantly, in all cases, the FC curve does not change when the measurements are repeated. This is expected in the Campbell regime for a state with a uniform distribution of vortex density. The irreversibility and difference between the ZFC and FC curves are also affected by vortex dynamics and reveal some interesting mechanisms of vortex creep through measurements of the time-dependent Campbell length [121].

For the pristine sample, Fig. 3(a),  $\lambda_C(T)$  is reversible for moderate magnetic fields. The hysteretic behavior between ZFC and FC  $\lambda_C$  appears above roughly 1.5 T. The ZFC develops a peak below  $T_c$ , indicating a rapid decrease in the persistent current. The two curves, ZFC-FC, merge at what is known as the “irreversibility” temperature, the subject of many previous

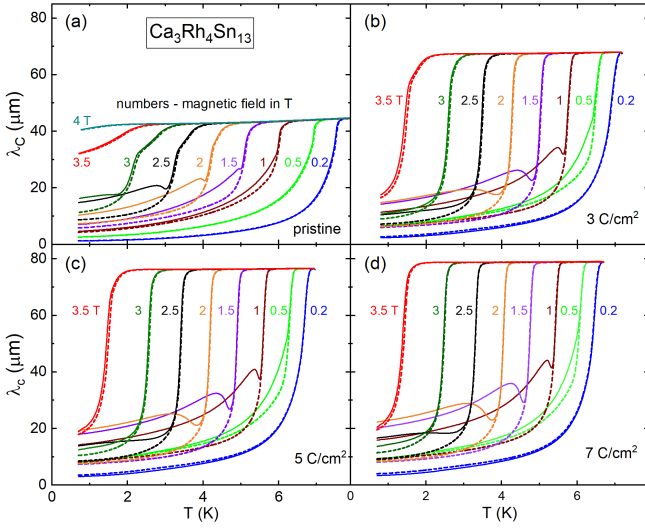


FIG. 3. Temperature variation of Campbell penetration depth,  $\lambda_C = \sqrt{\lambda_m^2 - \lambda_L^2}$ , measured at different DC magnetic fields applied parallel to the  $c$ -axis in (a) pristine, (b) electron irradiated at  $3 \text{ C}/\text{cm}^2$  dose, (c)  $5 \text{ C}/\text{cm}^2$ , and (d)  $7 \text{ C}/\text{cm}^2$ . The solid lines correspond to the ZFC protocol, and the dashed lines show FC data. The vertical and horizontal scales are the same for each graph.

works [38, 65, 122]. The height of the peak in the ZFC curves increases with the DC field magnitude. Similarly, a peak feature has been reported from low-frequency ( $H_{AC} = 1 \text{ Oe}$  and  $f = 211 \text{ Hz}$ ) AC susceptibility measurements in single crystals of  $\text{Ca}_3\text{Rh}_4\text{Sn}_{13}$ , which was interpreted as the order-disorder transition [123]. However, these measurements show complicated behavior, with the ZFC-FC lines crossing and a significant hysteresis between the FCW and FCC curves.

To further our understanding of the nature of the peak effect, it is important to examine the effect of controlled disorder. To do this without comparing different samples, the same sample was irradiated three times. The results are shown in Fig. 3(b,c,d). Upon irradiation, the peak feature appears at the lower magnetic fields and becomes significantly more prominent upon irradiation, exhibiting a larger difference between ZFC and FC curves. For example, at  $B = 1 \text{ T}$ , the peak in  $\lambda_{C,ZFC}(T)$  is absent in the pristine state but appears right after the first dose of  $3 \text{ C}/\text{cm}^2$  and becomes more prominent for higher doses. Clearly, electron irradiation introduces additional pinning and perhaps influences the pinning potential shape.

Figure 4 compares  $\lambda_C$  on the same graph. The main panel shows the ZFC (solid lines) and FC (dashed lines) curves measured at  $B = 1 \text{ T}$  for the pristine (blue lines) and for the maximum electron irradiation dose,  $7 \text{ C}/\text{cm}^2$  (red line). Since the critical temperature,  $T_c$ , is affected by irradiation [90] as shown in Fig. 1, the abscissa of Fig. 4 is normalized as  $T/T_c(H = 0)$ . The inset in Fig. 4 shows the size of the hysteresis,  $\lambda_{C,ZFC} - \lambda_{C,FC}$  evaluated at  $T = 0.8 \text{ K}$  plotted as a function of a magnetic

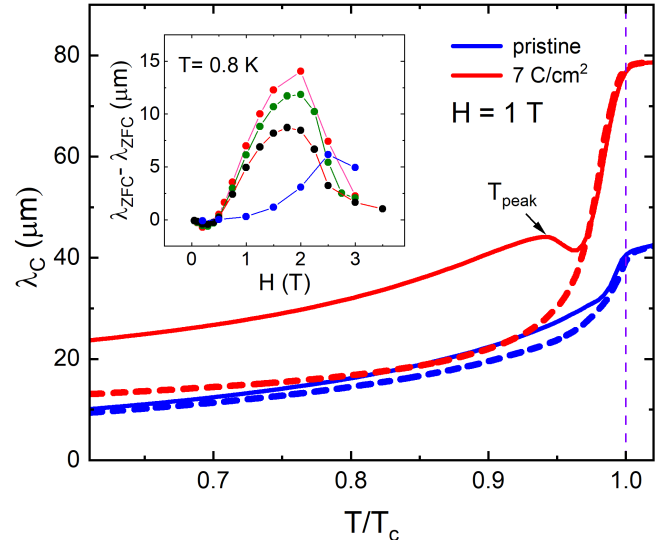


FIG. 4. Comparing the Campbell penetration depth,  $\lambda_C$ , for different irradiation doses. The main panel shows the temperature dependence of  $\lambda_C(T/T_c)$ , measured at  $B = 1 \text{ T}$  in pristine state and after electron irradiation  $7 \text{ C}/\text{cm}^2$ , demonstrating the significant effect of irradiation. Solid lines show ZFC data, and dashed lines show FC data. Inset: magnetic field dependence of the difference,  $\lambda_{C,ZFC} - \lambda_{C,FC}$  at  $T = 0.8 \text{ K}$ .

field. This hysteresis is larger in absolute numbers, than, for example, that observed in  $\text{Bi}_2\text{Sr}_2\text{CaCu}_2\text{O}_{\delta+y}$  crystals [102]. As expected, the hysteresis increases with the dose signaling a larger current density, leading to a larger bias of vortices in the non-parabolic potential wells.

## E. Critical current density

Finally, we evaluate the critical current density from Eq. 2 using the measured  $\lambda_C(T, B)$ , Fig. 3, and the coherence length,  $\xi = \sqrt{\phi_0/2\pi H_{c2}}$ , as a proxy for  $r_p$ . It is important to reiterate that the critical current density is obtained as a parameter contained in the equilibrium field-cooled value of the Campbell length, not from the vortex density gradient, which provides the persistent (relaxed) current density. The Helfand and Werthamer theory [124] fit of the upper critical field yields  $H_{c2}(0) = 3.9 \text{ T}$ , which gives,  $\xi(0) \approx 9.2 \text{ nm}$ . With  $\lambda_{c,FC}(T = 0.8 \text{ K}, B)$  from an isothermal slice at  $T = 0.8 \text{ K}$  of the data shown in Fig. 3, the field-dependent critical current density,  $j_c$ , is shown in Fig. 5 for the pristine and irradiated states of the same sample. While in the pristine state  $j_c(H)$  is a monotonically decreasing function, the curves after irradiation exhibit a pronounced peak effect at around  $2.0\text{--}2.5 \text{ T}$  at  $0.8 \text{ K}$ . When the same analysis is performed at other temperatures, we find that the peak shifts towards the lower fields, and its height decreases.

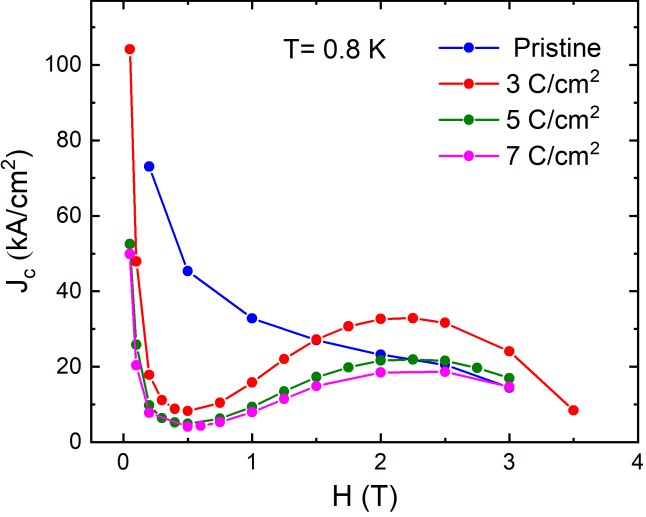


FIG. 5. Magnetic field dependence of the critical current density,  $j_c$ , estimated from  $\lambda_C(H)$  using Eq.3 for pristine and irradiated samples. A pronounced peak effect is induced by added disorder at large fields, but irradiation suppresses the critical current at small fields.

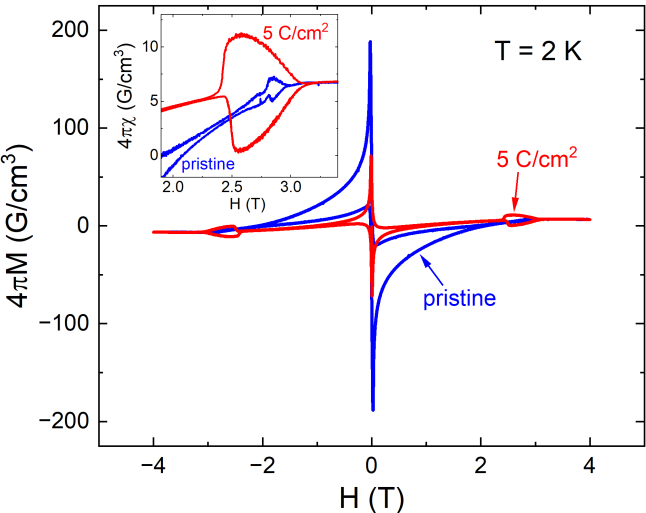


FIG. 6. Magnetization hysteresis loops measured using *Quantum Design* vibrating sample magnetometer (VSM) at  $T = 2$  K. Blue curves show a pristine state, and red curves show the data after electron irradiation with the dose of  $5 \text{ C}/\text{cm}^2$ . The inset zooms in at the region of a pronounced peak effect.

#### F. DC magnetic measurements

An unusual finding specific to this system is that, at low fields, the amplitude of the critical current density decreases with increasing irradiation dose. In most superconductors, the opposite is true. In order to verify that this is not an artifact, conventional magnetization was measured on the same sample using *Quantum Design* vibrating sample magnetometer (VSM). Figure. 6 shows  $M(H)$  hysteresis loops for the same sample in pristine

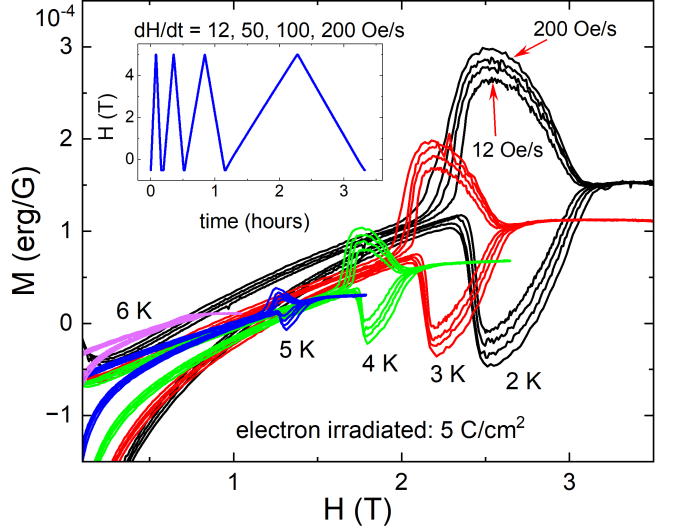


FIG. 7. Study of vortex dynamics measuring  $M(H)$  loops at different sweep rates,  $dH/dt = 12, 50, 100, 200 \text{ Oe/s}$  in the sample after  $5 \text{ C}/\text{cm}^2$  electron irradiation. As shown by red arrows, the inner-most curves are for the slowest rate of  $12 \text{ Oe/s}$ . The measurements were performed at  $2$  K (black),  $3$  K (red),  $4$  K (green),  $5$  K (blue) and  $6$  K (orange). The inset shows the time dependence of the applied magnetic field. Note that we used raw data to show the temperature-dependent background.

(blue lines) and after  $5 \text{ C}/\text{cm}^2$  electron irradiation (red curves). The inset zooms in on the region of a pronounced peak effect developed at fields close to  $H_{c2}$ . A small peak effect observed in the magnetization loops of a pristine sample indicates that dynamic effects are still present. Noticeable magnetic relaxation is substantial even at the lowest temperature. In the peak effect region, irradiation significantly enhances hysteresis. In lower fields, the hysteresis is reduced. This is consistent with Campbell length measurements, which are shown in Fig. 5.

Since we focus on both static and dynamic effects, it is important to check the effects of vortex relaxation. To probe the vortex dynamics at different magnetic fields, magnetization was measured at different sweep rates. Figure 7 shows the  $M(H)$  loops measured at  $2, 3, 4, 5$ , and  $6$  K in the sample after  $5 \text{ C}/\text{cm}^2$  electron irradiation. At each temperature, four loops were recorded at  $dH/dt = 12, 50, 100$ , and  $200 \text{ Oe/s}$ . Note that we used raw data, which show the temperature-dependent background, which does not affect our conclusions. The red arrows show that the inner-most curves correspond to the slowest rate of  $12 \text{ Oe/s}$  and the outer-most curves correspond to the fastest rate of  $200 \text{ Oe/s}$ . The inset shows the time dependence of the applied magnetic field. A steep, almost step-like increase in the  $M(H)$  amplitude at vortex entry (up sweeps) and the fact that this fishtail shape remains in the same field indicate a distinct vortex phase with its own critical current and relaxation dynamics. The different vortex phases for low and high fields were suggested for various superconduc-

tors [17, 18, 25, 28, 30, 38, 81]. In fact, the appearance of the hysteretic peak effect in our case is similar to electron irradiated  $MgB_2$  [81].

### G. Vortex phase diagram

We now construct the magnetic field - temperature phase diagram mapping the peak effect location line from Campbell length and from VSM magnetization measurements. As noted in the introduction, another 3-4-13 compound,  $Yb_3Rh_4Sn_{13}$ , exhibits a very similar vortex phase diagram [97, 98] suggesting that the features discussed here are not specific to  $Ca_3Rh_4Sn_{13}$ . Figure 8 shows the upper critical field defined as the onset temperature of the  $\lambda(T)$  curves for the pristine state (blue stars) and  $5 C/cm^2$  electron irradiated (green stars). For the latter, we also show magnetization (violet pentagons). The resulting  $H_{c2}(T)$  lines are close. In principle, non-magnetic scattering increases the  $H_{c2}$  [125], but unconventional superconductivity, here revealed by a substantial  $T_c$  reduction, may compensate that trend [90]. The red curve is the fit to the Helfand and Werthamer (HW) theory [124] using a universal scaling function [126], which yields  $H_{c2}(0) = 3.9 T$ .

Next, we explore the location of the peak effect at different temperatures. Squares (black - pristine, red - irradiated) show the peak location from VSM measurements of  $M(H)$  loops, whereas circles (green - pristine, orange - irradiated) show the peak location from Campbell length measurements of  $j_c(H)$ . The peak positions are somewhat shifted to lower values after irradiation but not significantly. The inset in Fig. 8 shows the inter-vortex distance at the peak location estimated for the triangular lattice,  $a = \sqrt{2\phi_0/\sqrt{3}B}$  and is in the range between 30 and 40 nm.

## IV. DISCUSSION

Our results show conclusively that non-magnetic point-like disorder can induce the peak effect in both the true unrelaxed critical current,  $j_c(H)$ , and in the relaxed persistent current,  $j(H)$ . The former was probed by the precision measurements of the Campbell penetration depth, and the latter was studied by conventional magnetization. Yet, the location of the peak effect on the magnetic field axis is practically the same. This firmly argues for the static origin of the peak effect in  $Ca_3Rh_4Sn_{13}$ .

This material itself has interesting vortex properties. The very low pinning is evident from the  $M(H)$  hysteresis loops, which are narrow and very asymmetric. The critical current density, obtained from the Campbell length, is in the range of  $2 - 7 \times 10^4 A/cm^2$  at low temperatures. It is likely that the vortex lattice is practically intact in pristine samples and follows the weak collective pinning with a monotonic magnetic field dependence of the

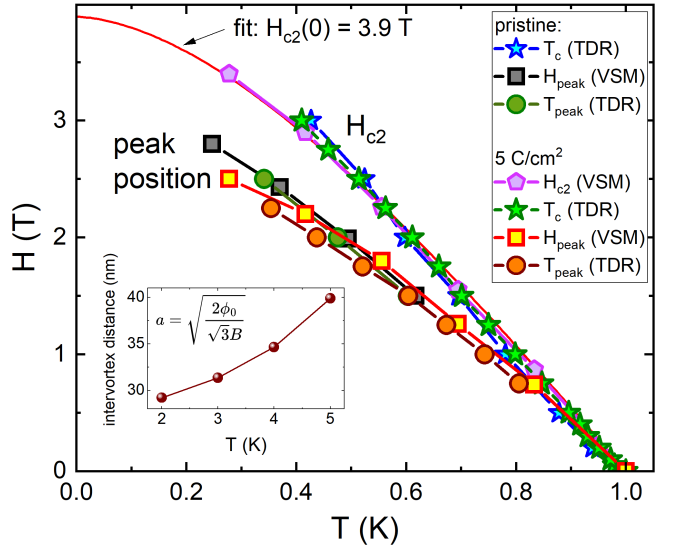


FIG. 8. Mixed state  $H(T)$  phase diagram of pristine and electron irradiated ( $5 C/cm^2$ ) states of the same crystal of  $Ca_3Rh_4Sn_{13}$  obtained from DC magnetization and Campbell penetration depth measurements. The upper critical field,  $H_{c2}$ , and the location of the peak effect feature are shown. The solid black line is fit to Helfand-Werthamer theory [124]. The inset shows the inter-vortex distance at the peak location estimated for the triangular lattice using the formula shown.

critical current. Irradiation disturbs the ordered lattice. The peak effect is already induced after the first dose of irradiation. Surprisingly, further irradiation appears to suppress the critical current density without affecting the peak position. It is possible that increased disorder suppresses the overall order parameter magnitude, thus reducing the condensation energy and reducing the strength of the elementary pinning forces. The suppression of the order parameter by irradiation is directly observed through the suppression of  $T_c$  shown in Fig. 1. An unconventional structure of the order parameter that fits this result was previously suggested [90]. Another, and a more realistic explanation, is that our assumption that  $r_p \approx \xi$  is not applicable. It is likely that  $r_p$  is larger, due to the collective effects and pinning of vortex bundles [2]. The bundle size grows with a magnetic field, and the effective pinning range is related to the correlated volume of the bundles. According to Eq.3, this will increase the estimate of the critical current density compared to a simplified single-vortex pinning regime.

The location of the peak corresponds to the inter-vortex distance that ranges from 30 to 40 nm, which is quite dense vortex lattice. Our results strongly support the scenario in which the peak effect is caused by a random point-like disorder that triggers a crossover from the collective pinning of vortex bundles to a disordered vortex phase. It is possible that in other systems the level of natural disorder is already high enough to cause such a crossover and exhibit a peak effect.

## V. CONCLUSION

In conclusion, Campbell penetration depth measurements were used to study the magnetic field-dependent unrelaxed critical current density,  $j_c(H)$ , for different levels of point-like non-magnetic disorder induced by 2.5 MeV electron irradiation. The behavior of the critical current density is monotonic in field in the pristine state. The lowest dose of electron irradiation already induces a pronounced peak effect in  $j_c(H)$ . The same peak is observed in complementary magnetization measurements. These results strongly support the static picture of the peak effect in  $\text{Ca}_3\text{Rh}_4\text{Sn}_{13}$ . Considering that  $\text{Ca}_3\text{Rh}_4\text{Sn}_{13}$  is a very low pinning superconductor in which the collective pinning model is likely applicable, the peak effect induced by a controlled disorder must be due to a crossover from an almost perfect lattice to a disordered vortex phase, as suggested in a number of prior works [21, 23, 25, 32, 36–38]. Having access to the unrelaxed critical current, we confirm this scenario of the peak effect formation.

## VI. ACKNOWLEDGEMENTS

We thank Kirill Kovnir for explaining that the often-used designation of the 3-4-13 compounds studied here as 'quasi-skutterudites' is incorrect. Instead, 'Remeika series' should be used. This work was supported by the National Science Foundation under Grant No. DMR-2219901. M.A.T. and K.R.J. were supported by the U.S. Department of Energy (DOE), Office of Science, Basic Energy Sciences, Materials Science and Engineering Division. Ames National Laboratory is operated for the U.S. DOE by Iowa State University under Contract No. DE-AC02-07CH11358. The authors acknowledge support from the EMIR&A French network (FR CNRS 3618) on the platform SIRIUS, proposals No. 20-5925 and 23-4663. Work at BNL (materials synthesis) was supported by the U.S. Department of Energy, Basic Energy Sciences, Division of Materials Science and Engineering, under Contract No. DE-SC0012704. C.P. acknowledges support from the Shanghai Key Laboratory of Material Frontiers Research in Extreme Environments, China (No. 22dz2260800) and Shanghai Science and Technology Committee, China (No. 22JC1410300).

---

[1] A. A. Abrikosov, On the Magnetic Properties of Superconductors of the Second Group, [ZhETF 32, 1442-1450 (1957)] Sov. Phys. JETP **5**, 1174 (1957).

[2] G. Blatter, M. V. Feigel'man, V. B. Geshkenbein, A. I. Larkin, and V. M. Vinokur, Vortices in high-temperature superconductors, Rev. Mod. Phys. **66**, 1125 (1994).

[3] E. H. Brandt, The flux-line lattice in superconductors, Rep. Prog. Phys. **58**, 1465 (1995).

[4] W.-K. Kwok, U. Welp, A. Glatz, A. E. Koshelev, K. J. Kihlstrom, and G. W. Crabtree, Vortices in high-performance high-temperature superconductors, Rep. Prog. Phys. **79**, 116501 (2016).

[5] S. Eley, A. Glatz, and R. Willa, Challenges and transformative opportunities in superconductor vortex physics, J. Appl. Phys. **130**, 050901 (2021).

[6] A. M. Campbell, The interaction distance between flux lines and pinning centres, J. Phys. C: Solid State Phys. **4**, 3186 (1971).

[7] D. Dew-Huges, Flux pinning mechanisms in type-II superconductors, Phil. Mag. **30**, 293 (1974).

[8] Y. Yeshurun, A. P. Malozemoff, and A. Shaulov, Magnetic relaxation in high-temperature superconductors, Reviews of Modern Physics **68**, 911 (1996).

[9] M. Tinkham, *Introduction to Superconductivity*, 2nd ed., Dover Books on Physics (Dover Publications, 2004).

[10] W. DeSorbo, The peak effect in substitutional and interstitial solid solutions of high-field superconductors, Rev. Mod. Phys. **36**, 90 (1964).

[11] A. B. Pippard, A possible mechanism for the peak effect in type II superconductors, Phil. Mag. **19**, 217 (1969).

[12] C. Van der Klein, P. Kes, and D. De Klerk, Peak effect in superconducting niobium, induced by neutron irradiation, Philos. Mag. **29**, 559 (1974).

[13] C. Tang, X. Ling, S. Bhattacharya, and P. M. Chaikin, Peak effect in superconductors: melting of larkin domains, Europhys. Lett. **35**, 597 (1996).

[14] C. Tomy, G. Balakrishnan, and D. M. Paul, Observation of the peak effect in the superconductor  $\text{Ca}_3\text{Rh}_4\text{Sn}_{13}$ , Phys. Rev. B **56**, 8346 (1997).

[15] S. Sarkar, S. Banerjee, A. Grover, S. Ramakrishnan, S. Bhattacharya, G. Ravikumar, P. Mishra, V. Sahni, C. Tomy, D. M. Paul, *et al.*, Peak effect in  $\text{Ca}_3\text{Rh}_4\text{Sn}_{13}$ : vortex phase diagram and evidences for stepwise amorphization of flux line lattice, Physica C **341**, 1085 (2000).

[16] H. R. Naren, A. Tamizhavel, S. Ramakrishnan, and A. K. Grover, Vortex phase diagram in weakly pinned  $\text{Rh}_{17}\text{S}_{15}$ , Journal of Physics: Conference Series **150**, 052183 (2009).

[17] M. S. Babu and D. Pal, Step change in equilibrium magnetization across the second magnetization peak and the peak effect region of a weakly pinned low  $T_c$  superconductor,  $\text{Ca}_3\text{Rh}_4\text{Sn}_{13}$ , Physica B **448**, 188 (2014).

[18] S. Kumar, V. Kushwaha, R. Singh, A. Thamizhavel, C. Tomy, and K. Grover, Elucidation of peak effect phenomenon in a single crystal of superconducting  $\text{Ca}_3\text{Ir}_4\text{Sn}_{13}$ , AIP Conf. Proc. **1665**, 130009 (2015).

[19] Z. F. Weng, M. Smidman, G. M. Pang, O. Prakash, Y. Chen, Y. J. Zhang, S. Ramakrishnan, and H. Q. Yuan, Nodeless superconductivity and the peak effect in the quasiskutterudites  $\text{Lu}_3\text{Os}_4\text{Ge}_{13}$  and  $\text{Y}_3\text{Ru}_4\text{Ge}_{13}$ , Phys. Rev. B **95**, 184501 (2017).

[20] S. Sarkar, D. Pal, S. S. Banerjee, S. Ramakrishnan, A. K. Grover, C. V. Tomy, G. Ravikumar, P. K. Mishra, V. C. Sahni, G. Balakrishnan, D. M. Paul, and S. Bhattacharya, Stepwise amorphization of the flux-line lattice in  $\text{Ca}_3\text{Rh}_4\text{Sn}_{13}$ : A peak-effect study, Phys. Rev. B **61**,

12394 (2000).

[21] T. Giamarchi and P. Le Doussal, Phase diagrams of flux lattices with disorder, *Phys. Rev. B* **55**, 6577 (1997).

[22] J. Kierfeld and V. Vinokur, Lindemann criterion and vortex lattice phase transitions in type-II superconductors, *Phys. Rev. B* **69**, 024501 (2004).

[23] G. Blatter, V. B. Geshkenbein, and J. A. G. Koopmann, Weak to strong pinning crossover, *Phys. Rev. Lett.* **92**, 067009 (2004).

[24] Y. Liu, L. Zhou, K. Sun, W. E. Straszheim, M. A. Tanatar, R. Prozorov, and T. A. Lograsso, Doping evolution of the second magnetization peak and magnetic relaxation in BaK122 single crystals, *Phys. Rev. B* **97**, 054511 (2018).

[25] M. Jirsa, L. Püst, D. Dlouhý, and M. R. Koblischka, Fishtail shape in the magnetic hysteresis loop for superconductors: Interplay between different pinning mechanisms, *Phys. Rev. B* **55**, 3276 (1997).

[26] G. P. Mikitik and E. H. Brandt, Peak effect, vortex-lattice melting line, and order-disorder transition in conventional and high- $T_c$  superconductors, *Phys. Rev. B* **64**, 184514 (2001).

[27] J. A. G. Koopmann, V. B. Geshkenbein, and G. Blatter, Peak effect at the weak to strong pinning crossover, *Physica C* **404**, 209 (2004).

[28] S. S. Banerjee, S. Ramakrishnan, A. K. Grover, G. Ravikumar, P. K. Mishra, V. C. Sahni, C. V. Tomy, G. Balakrishnan, D. M. Paul, P. L. Gammel, D. J. Bishop, E. Bucher, M. J. Higgins, and S. Bhattacharya, Peak effect, plateau effect, and fishtail anomaly: The reentrant amorphization of vortex matter in 2H-NbSe<sub>2</sub>, *Phys. Rev. B* **62**, 11838 (2000), times Cited: 22.

[29] R. Prozorov, M. A. Tanatar, E. C. Blomberg, P. Prommapan, R. T. Gordon, N. Ni, S. L. Bud'ko, and P. C. Canfield, Doping - Dependent irreversible magnetic properties of Ba(Fe<sub>1-x</sub>Co<sub>x</sub>)<sub>2</sub>As<sub>2</sub> single crystals, *Physica C* **469**, 667 (2009).

[30] L. Gao, T. Ying, Y. Zhao, W. Cao, C. Li, L. Xiong, Q. Wang, C. Pei, J.-Y. Ge, H. Hosono, and Y. Qi, Fishtail effect and the vortex phase diagram of high-entropy alloy superconductor, *Appl. Phys. Lett.* **120**, 092602 (2022).

[31] M. Daeumling, J. M. Seuntjens, and D. C. Larbalestier, Oxygen-defect flux pinning, anomalous magnetization and intra-grain granularity in YBa<sub>2</sub>Cu<sub>3</sub>O<sub>7-δ</sub>, *Nature* **346**, 332 (1990).

[32] D. Giller, A. Shaulov, R. Prozorov, Y. Abulafia, Y. Wolfs, L. Burlachkov, Y. Yeshurun, E. Zeldov, V. M. Vinokur, J. L. Peng, and R. L. Greene, Disorder-induced transition to entangled vortex solid in Nd-Ce-Cu-O crystal, *Phys. Rev. Lett.* **79**, 2542 (1997).

[33] L. Klein, E. R. Yacoby, Y. Yeshurun, A. Erb, G. Müller-Vogt, V. Breit, and H. Wühl, Peak effect and scaling of irreversible properties in untwinned Y-Ba-Cu-O crystals, *Phys. Rev. B* **49**, 4403 (1994).

[34] L. Krusin-Elbaum, L. Civale, V. M. Vinokur, and F. Holtzberg, “Phase diagram” of the vortex-solid phase in Y-Ba-Cu-O crystals: A crossover from single-vortex (1D) to collective (3D) pinning regimes, *Phys. Rev. Lett.* **69**, 2280 (1992).

[35] T. Matsushita, Measurement methods for critical current density, in *Flux Pinning in Superconductors* (Springer, 2022) pp. 205–226.

[36] R. Willa, A. E. Koshelev, I. A. Sadovskyy, and A. Glatz, Peak effect due to competing vortex ground states in superconductors with large inclusions, *Phys. Rev. B* **98**, 054517 (2018).

[37] Y. Abulafia, A. Shaulov, Y. Wolfus, R. Prozorov, L. Burlachkov, Y. Yeshurun, D. Majer, E. Zeldov, H. Wühl, V. B. Geshkenbein, and V. M. Vinokur, Plastic vortex creep in YBa<sub>2</sub>Cu<sub>3</sub>O<sub>7-x</sub> crystals, *Phys. Rev. Lett.* **77**, 1596 (1996).

[38] M. Konczykowski, F. Rullier-Albenque, Y. Yeshurun, E. Yacoby, A. Shaulov, and J. Gilchrist, Effects of electron irradiation on irreversibility line in superconducting YBa<sub>2</sub>Cu<sub>3</sub>O<sub>7</sub>, *Supercond. Sci. Technol.* **4**, S445 (1991).

[39] P. Fulde and R. A. Ferrell, Superconductivity in a Strong Spin-Exchange Field, *Phys. Rev.* **135**, A550 (1964).

[40] A. Larkin and Y. N. Ovchinnikov, Nonuniform state of superconductors, *Soviet Physics-JETP* **20**, 762 (1965).

[41] M. Tachiki, S. Takahashi, P. Gegenwart, M. Weiden, M. Lang, C. Geibel, F. Steglich, R. Modler, C. Paulsen, and Y. Ōnuki, Generalized Fulde-Ferrell-Larkin-Ovchinnikov state in heavy-fermion and intermediate-valence systems, *Zeitschrift für Physik B Condensed Matter* **100**, 369 (1997).

[42] M. Tachiki, T. Koyama, and S. Takahashi, Some exotic phenomena related to vortices in high-T<sub>c</sub> and heavy fermion superconductors, *Physica C: Superconductivity* **263**, 1 (1996).

[43] M. Houzet, Y. Meurdsoif, O. Coste, and A. Buzdin, Structure of the non-uniform fulde-ferrell-larkin-ovchinnikov state in 3d superconductors, *Physica C* **316**, 89 (1999).

[44] P. Gegenwart, M. Deppe, M. Köppen, F. Kromer, M. Lang, R. Modler, M. Weiden, C. Geibel, F. Steglich, T. Fukase, *et al.*, Anomalous peak effect in heavy-fermion, intermediate-valence and A15 superconductors: Evidence for a Fulde-Ferrell-Larkin-Ovchinnikov state?, *Annalen der Physik* **508**, 307 (1996).

[45] K. Gloos, R. Modler, H. Schimanski, C. D. Bredl, C. Geibel, F. Steglich, A. I. Buzdin, N. Sato, and T. Komatsubara, Possible formation of a nonuniform superconducting state in the heavy-fermion compound UPd<sub>2</sub>Al<sub>3</sub>, *Phys. Rev. Lett.* **70**, 501 (1993).

[46] H. Yaguchi, T. Akima, Z. Mao, Y. Maeno, and T. Ishiguro, Detailed study of the ac susceptibility of Sr<sub>2</sub>RuO<sub>4</sub> in oriented magnetic fields, *Phys. Rev. B* **66**, 214514 (2002).

[47] M. A. Tanatar, S. Nagai, Z. Q. Mao, Y. Maeno, and T. Ishiguro, Thermal conductivity of superconducting Sr<sub>2</sub>RuO<sub>4</sub> in oriented magnetic fields, *Phys. Rev. B* **63**, 064505 (2001).

[48] K. Deguchi, M. A. Tanatar, Z. Mao, T. Ishiguro, and Y. Maeno, Superconducting double transition and the upper critical field limit of Sr<sub>2</sub>RuO<sub>4</sub> in parallel magnetic fields, *Journal of the Physical Society of Japan* **71**, 2839 (2002), <https://doi.org/10.1143/JPSJ.71.2839>.

[49] V. Ferrando, M. Affronte, D. Daghero, R. Di Capua, C. Tarantini, and M. Putti, Neutron irradiation effects on two gaps in MgB<sub>2</sub>, *Physica C* **456**, 144 (2007).

[50] C. Tarantini, M. Putti, A. Gurevich, Y. Shen, R. K. Singh, J. M. Rowell, N. Newman, D. C. Larbalestier, P. Cheng, Y. Jia, and H.-H. Wen, Suppression of the Critical Temperature of Superconducting NdFeAs(O)F

Single Crystals by Kondo-Like Defect Sites Induced by  $\alpha$ -Particle Irradiation, *Phys. Rev. Lett.* **104**, 087002 (2010).

[51] T. Taen, F. Ohtake, H. Akiyama, H. Inoue, Y. Sun, S. Pyon, T. Tamegai, and H. Kitamura, Pair-breaking effects induced by 3-MeV proton irradiation in BaK122, *Phys. Rev. B* **88**, 224514 (2013).

[52] R. Prozorov, M. Kończykowski, M. A. Tanatar, A. Thaler, S. L. Bud'ko, P. C. Canfield, V. Mishra, and P. J. Hirschfeld, Effect of Electron Irradiation on Superconductivity in Single Crystals of  $\text{Ba}(\text{Fe}_{1-x}\text{Ru}_x)_2\text{As}_2$  ( $x = 0.24$ ), *Phys. Rev. X* **4**, 041032 (2014).

[53] S. L. Bud'ko and P. C. Canfield, Superconductivity of magnesium diboride, *Physica C* **514**, 142 (2015).

[54] M. Moroni, L. Gozzelino, G. Ghigo, M. A. Tanatar, R. Prozorov, P. C. Canfield, and P. Carretta, Effect of proton irradiation on the normal-state low-energy excitations of  $\text{Ba}(\text{Fe}_{1-x}\text{Rh}_x)_2\text{As}_2$  superconductors, *Phys. Rev. B* **96**, 094523 (2017).

[55] K. Cho, M. Kończykowski, S. Teknowijoyo, M. A. Tanatar, and R. Prozorov, Using electron irradiation to probe iron-based superconductors, *Superc. Sci. Technol.* **31**, 064002 (2018).

[56] G. Ghigo, D. Torsello, G. A. Ummarino, L. Gozzelino, M. A. Tanatar, R. Prozorov, and P. C. Canfield, Disorder-Driven Transition from  $s_{\pm}$  to  $s_{++}$  Superconducting Order Parameter in Proton Irradiated  $\text{Ba}(\text{Fe}_{1-x}\text{Rh}_x)_2\text{As}_2$  Single Crystals, *Phys. Rev. Lett.* **121**, 107001 (2018).

[57] D. Torsello, G. Ummarino, J. Bekaert, L. Gozzelino, R. Gerbaldo, M. Tanatar, P. Canfield, R. Prozorov, and G. Ghigo, Tuning the Intrinsic Anisotropy with Disorder in the CaKFe<sub>4</sub>As<sub>4</sub> Superconductor, *Phys. Rev. Applied* **13**, 064046 (2020).

[58] E. I. Timmons, S. Teknowijoyo, M. Kończykowski, O. Cavani, M. A. Tanatar, S. Ghimire, K. Cho, Y. Lee, L. Ke, N. H. Jo, S. L. Bud'ko, P. C. Canfield, P. P. Orth, M. S. Scheurer, and R. Prozorov, Electron irradiation effects on superconductivity in PdTe<sub>2</sub>: An application of a generalized Anderson theorem, *Phys. Rev. Research* **2**, 023140 (2020).

[59] M. A. Tanatar, D. Torsello, K. R. Joshi, S. Ghimire, C. J. Kopas, J. Marshall, J. Y. Mutus, G. Ghigo, M. Zarea, J. A. Sauls, and R. Prozorov, Anisotropic superconductivity of niobium based on its response to nonmagnetic disorder, *Phys. Rev. B* **106**, 224511 (2022).

[60] W. Li, S. Pyon, A. Yagi, T. Ren, M. Suyama, J. Wang, T. Matsumae, Y. Kobayashi, A. Takahashi, D. Miyawaki, and T. Tamegai, Effects of 3 MeV Proton Irradiation on Superconductivity and CDW in 2H-NbSe<sub>2</sub> Single Crystals, *J. Phys. Soc. Jpn.* **92**, 064701 (2023).

[61] R. Wilke, P. Samuely, P. Szabó, Z. Ho Ľanová, S. Bud'ko, P. Canfield, and D. Finnemore, Superconducting and normal state properties of carbon doped and neutron irradiated MgB<sub>2</sub>, *Physica C* **456**, 108 (2007).

[62] C. Krutzler, M. Zehetmayer, M. Eisterer, H. Weber, N. Zhigadlo, and J. Karpinski, Comparative study of neutron irradiation and carbon doping in MgB<sub>2</sub> single crystals, *Phys. Rev. B* **75**, 224510 (2007).

[63] A. Ślebarski, P. Zajdel, M. Fijalkowski, M. M. Maska, P. Witas, J. Goraus, Y. Fang, D. C. Arnold, and M. B. Maple, The effective increase in atomic scale disorder by doping and superconductivity in Ca<sub>3</sub>Rh<sub>4</sub>Sn<sub>13</sub>, *New J. Phys.* **20**, 103020 (2018).

[64] M. Chung, Y.-K. Kuo, Z. Xu, L. DeLong, J. Brill, and R. Budhani, Effects of transport current and columnar defects on the rf penetration depth of NbSe<sub>2</sub>, *Phys. Rev. B* **50**, 1329 (1994).

[65] R. Prozorov, M. Konczykowski, B. Schmidt, Y. Yeshev, A. Shaulov, C. Villard, and G. Koren, Origin of the irreversibility line in thin  $\text{YBa}_2\text{Cu}_3\text{O}_{7-\delta}$  films with and without columnar defects, *Phys. Rev. B* **54**, 15530 (1996).

[66] A. Mazilu, H. Safar, M. P. Maley, J. Y. Coulter, L. N. Bulaevskii, and S. Foltyn, Vortex dynamics of heavy-ion-irradiated  $\text{YBa}_2\text{Cu}_3\text{O}_{7-\delta}$ : Experimental evidence for a reduced vortex mobility at the matching field, *Phys. Rev. B* **58**, R8909 (1998).

[67] G. Pasquini, L. Civale, H. Lanza, and G. Nieva, Dynamic regimes in the ac response of  $\text{YBa}_2\text{Cu}_3\text{O}_7$  with columnar defects: Intra- and inter-valley vortex motion, *Phys. Rev. B* **59**, 9627 (1999).

[68] N. Chikumoto, M. Konczykowski, T. Terai, and M. Murakami, Modification of flux pinning properties of RE-Ba-Cu-O superconductor by irradiation, *Supercond. Sci. Technol.* **13**, 749 (2000).

[69] N. Chikumoto, A. Yamamoto, M. Konczykowski, and M. Murakami, Magnetization behavior of MgB<sub>2</sub> and the effect of high energy heavy-ion irradiation, *Physica C* **378-381**, 466 (2002).

[70] L. Civale, A. V. Silhanek, and G. Pasquini, Angular dependent vortex dynamics in superconductors with columnar defects., *Stud. High Temp. Supercond.* **47**, 41 (2003).

[71] C. Marcenat, S. Blanchard, J. Marcus, L. M. Paulius, C. J. van der Beek, M. Konczykowski, and T. Klein, Anisotropic Enhancement of Superconductivity in Heavy-Ion Irradiated (K,Ba)BiO<sub>3</sub>, *Phys. Rev. Lett.* **90**, 037004 (2003).

[72] M. Haruta, T. Fujiyoshi, T. Sueyoshi, K. Miyahara, T. Ikegami, K. Ebihara, R. Miyagawa, N. Ishikawa, S. Awaji, and K. Watanabe, Influence of columnar defects on pinning parameters in high- $T_c$  superconductors, *Physica C* **412-414**, 511 (2004).

[73] Y. Nakajima, Y. Tsuchiya, T. Taen, T. Tamegai, S. Okayasu, and M. Sasase, Enhancement of critical current density in Co-doped BaFe<sub>2</sub>As<sub>2</sub> with columnar defects introduced by heavy-ion irradiation, *Phys. Rev. B* **80**, 012510 (2009).

[74] Y. Nakajima, T. Taen, Y. Tsuchiya, T. Tamegai, H. Kitamura, and T. Murakami, Suppression of the critical temperature of superconducting  $\text{Ba}(\text{Fe}_{1-x}\text{Co}_x)_2\text{As}_2$  by point defects from proton irradiation, *Phys. Rev. B* **82**, 220504 (2010).

[75] L. Fang, Y. Jia, J. A. Schlueter, A. Kayani, Z. L. Xiao, H. Claus, U. Welp, A. E. Koshelev, G. W. Crabtree, and W. Kwok, Doping- and irradiation-controlled pinning of vortices in BaFe<sub>2</sub>(As<sub>1-x</sub>P<sub>x</sub>)<sub>2</sub> single crystals, *Phys. Rev. B* **84**, 140504 (2011).

[76] N. Haberkorn, B. Maiorov, I. O. Usov, M. Weigand, W. Hirata, S. Miyasaka, S. Tajima, N. Chikumoto, K. Tanabe, and L. Civale, Influence of random point defects introduced by proton irradiation on critical current density and vortex dynamics of  $\text{Ba}(\text{Fe}_{0.925}\text{Co}_{0.075})_2\text{As}_2$  single crystals, *Phys. Rev. B* **85**, 014522 (2012).

[77] N. Haberkorn, J. Kim, S. Suárez, J.-H. Lee, and S. H. Moon, Influence of random point defects introduced by proton irradiation on the flux creep rates and magnetic field dependence of the critical current, *Supercond. Sci. Technol.* **28**, 125007 (2015).

[78] Y. Radzyner, A. Shaulov, Y. Yeshurun, K. Kishio, and S. Okayasu, Effects of electron irradiation on the vortex order-disorder transition in  $\text{La}_{2-x}\text{Sr}_x\text{CuO}_4$  crystals, *Physica C* **388-389**, 753 (2003).

[79] A. A. Blinkin, V. V. Derevyanko, A. N. Dovbnya, T. V. Sukhareva, V. A. Finkel', and I. N. Shlyakhov, Effect of electron irradiation on the structure and properties of the  $\text{MgB}_2$  superconductor, *Physics of the Solid State* **48**, 2037 (2006).

[80] E. Bartolomé, J. Bartolomé, A. Arauzo, V. Eremenko, and V. Sirenko, AC response of  $2\text{H}-\text{NbSe}_2$  single crystals with electron-irradiation-induced defects, *J. Phys. Condens. Matter* **22**, 295702 (2010).

[81] T. Klein, R. Marlaud, C. Marcenat, H. Cercellier, M. Konczykowski, C. J. van der Beek, V. Mosser, H. S. Lee, and S. I. Lee, First-Order Transition in the Magnetic Vortex Matter in Superconducting  $\text{MgB}_2$  Tuned by Disorder, *Phys. Rev. Lett.* **105**, 047001 (2010).

[82] C. J. van der Beek, S. Demirdiç, D. Colson, F. Rullier-Albenque, Y. Fasano, T. Shibauchi, Y. Matsuda, S. Kasahara, P. Gierlowski, and M. Konczykowski, Electron irradiation of Co, Ni, and P-doped  $\text{BaFe}_2\text{As}_2$ -type iron-based superconductors, *J. Phys.: Conf. Ser.* **449**, 012023 (2013).

[83] R. Meier-Hirmer and H. Küpfer, Influence of neutron radiation induced defects on the superconducting properties of  $\text{V}_3\text{Si}$ , *J. Nucl. Mater.* **108-109**, 593 (1982).

[84] M. Eisterer, Influence of disorder on  $\text{H}_{c2}$ -anisotropy and flux pinning in  $\text{MgB}_2$ , *physica status solidi (c)* **2**, 1606 (2005).

[85] R. H. T. Wilke, S. L. Bud'ko, P. C. Canfield, J. Farmer, and S. T. Hannahs, Systematic study of the superconducting and normal-state properties of neutron-irradiated  $\text{MgB}_2$ , *Phys. Rev. B* **73**, 134512 (2006).

[86] M. Putti, R. Vaglio, and J. M. Rowell, Radiation effects on  $\text{MgB}_2$ : a review and a comparison with A15 superconductors, *Superc. Sci. Technol.* **21**, 043001 (2008).

[87] A. E. Karkin, T. Wolf, and B. N. Goshchitskii, Superconducting properties of  $(\text{BaK})\text{Fe}_2\text{As}_2$  single crystals disordered with fast neutron irradiation, *J. Phys. Cond. Matt.* **26**, 275702 (2014).

[88] H. Chauhan and G. D. Varma, Effects of gamma-irradiation on the superconducting properties of  $\text{FeTe}_{0.55}\text{Se}_{0.45}$  single crystals grown by self-flux method, *J. App. Phys.* **135**, 113901 (2024).

[89] C. Tarantini, K. Iida, N. Sumiya, M. Chihara, T. Hatano, H. Ikuta, R. K. Singh, N. Newman, and D. C. Larbalestier, Effect of  $\alpha$ -particle irradiation on a  $\text{NdFeAs(O,F)}$  thin film, *Superc. Sci. Technol.* **31**, 034002 (2018).

[90] E. H. Krenkel, M. A. Tanatar, M. Kończykowski, R. Grasset, E. I. Timmons, S. Ghimire, K. R. Joshi, Y. Lee, L. Ke, S. Chen, C. Petrovic, P. P. Orth, M. S. Scheurer, and R. Prozorov, Possible unconventional pairing in  $(\text{Ca},\text{Sr})_3(\text{Ir},\text{Rh})_4\text{Sn}_{13}$  superconductors revealed by controlling disorder, *Phys. Rev. B* **105**, 094521 (2022).

[91] E. Krenkel, M. Tanatar, S. Ghimire, K. Joshi, S. Chen, C. Petrovic, and R. Prozorov, Robust superconductivity and the suppression of charge-density wave in the quasi-skutterudites  $\text{Ca}_3(\text{Ir}_{1-x}\text{Rh}_x)_4\text{Sn}_{13}$  single crystals at ambient pressure, *Journal of Physics: Condensed Matter* **36** (2024).

[92] J. P. Remeika, G. P. Espinosa, A. S. Cooper, H. Barz, J. M. Rowell, D. B. McWhan, J. M. Vandenberg, D. E. Moncton, Z. Fisk, L. D. Woolf, H. C. Hamaker, M. B. Maple, G. Shirane, and W. Thomlinson, A new family of ternary intermetallic superconducting/magnetic stannides, *Solid State Comm.* **34**, 923 (1980).

[93] R. Gumeniuk, Chapter 304 - structural and physical properties of remeika phases, in *Including Actinides, Handbook on the Physics and Chemistry of Rare Earths*, Vol. 54, edited by J.-C. G. Bünzli and V. K. Pecharsky (Elsevier, 2018) pp. 43-143.

[94] S. K. Goh, D. A. Tompsett, P. J. Saines, H. C. Chang, T. Matsumoto, M. Imai, K. Yoshimura, and F. M. Grosche, Ambient Pressure Structural Quantum Critical Point in the Phase Diagram of  $(\text{Sr}_{1-x}\text{Ca}_x)_3\text{Rh}_4\text{Sn}_{13}$ , *Phys. Rev. Lett.* **114**, 097002 (2015).

[95] W. C. Yu, Y. W. Cheung, P. J. Saines, M. Imai, T. Matsumoto, C. Michioka, K. Yoshimura, and S. K. Goh, Strong Coupling Superconductivity in the Vicinity of the Structural Quantum Critical Point in  $(\text{Ca}_x\text{Sr}_{1-x})_3\text{Rh}_4\text{Sn}_{13}$ , *Phys. Rev. Lett.* **115**, 207003 (2015).

[96] S. Kumar, R. P. Singh, A. Thamizhavel, C. Tomy, and A. Grover, Vortex phase diagram study in the superconductor  $\text{Ca}_3\text{Ir}_4\text{Sn}_{13}$ , *Mater. Res. Express* **5**, 106002 (2018).

[97] H. Sato, Y. Aoki, H. Sugawara, and T. Fukuhara, Peak effect in the superconducting mixed state of  $\text{Yb}_3\text{Rh}_4\text{Sn}_{13}$  single crystals, *Journal of the Physical Society of Japan* **64**, 3175 (1995).

[98] C. Tomy, G. Balakrishnan, and D. M. Paul, Regions of enhanced pinning in the mixed state of the superconductor  $\text{Yb}_3\text{Rh}_4\text{Sn}_{13}$ , *Physica C: Superconductivity* **280**, 1 (1997).

[99] K. Wang and C. Petrovic,  $\text{Ca}_3\text{Ir}_4\text{Sn}_{13}$ : A weakly correlated nodeless superconductor, *Phys. Rev. B* **86**, 024522 (2012).

[100] M. A. Tanatar, N. Ni, S. L. Bud'ko, P. C. Canfield, and R. Prozorov, Field-dependent transport critical current in single crystals of  $\text{Ba}(\text{Fe}_{1-x}\text{TM}_x)_2\text{As}_2$  ( $\text{TM} = \text{Co}, \text{Ni}$ ) superconductors, *Supercond. Sci. Technol.* **23**, 054002 (2010).

[101] R. Prozorov, R. W. Giannetta, A. Carrington, P. Fournier, R. L. Greene, P. Guptasarma, D. G. Hinks, and A. R. Banks, Measurements of the absolute value of the penetration depth in high-Tc superconductors using a low-Tc superconductive coating, *Appl. Phys. Lett.* **77**, 4202 (2000).

[102] R. Prozorov, R. W. Giannetta, N. Kameda, T. Tamegai, J. A. Schlueter, and P. Fournier, Campbell penetration depth of a superconductor in the critical state, *Phys. Rev. B* **67**, 184501 (2003).

[103] R. Giannetta, A. Carrington, and R. Prozorov, London Penetration Depth Measurements Using Tunnel Diode Resonators, *J. Low Temp. Phys.* **208**, 119-146 (2022).

[104] R. Prozorov, Meissner-London Susceptibility of Superconducting Right Circular Cylinders in an Axial Magnetic Field, *Phys. Rev. Applied* **16**, 024014 (2021).

[105] R. T. Gordon, H. Kim, N. Salovich, R. W. Giannetta, R. M. Fernandes, V. G. Kogan, T. Prozorov, S. L. Bud'ko, P. C. Canfield, M. A. Tanatar, and R. Pro-

zorov, Doping evolution of the absolute value of the London penetration depth and superfluid density in single crystals of  $\text{Ba}(\text{Fe}_{1-x}\text{Co}_x)_2\text{As}_2$ , *Phys. Rev. B* **82**, 054507 (2010).

[106]A. E. Koshelev and V. M. Vinokur, Frequency response of pinned vortex lattice, *Physica C* **173**, 465 (1991).

[107]R. Willa, V. B. Geshkenbein, and G. Blatter, Campbell penetration in the critical state of type-II superconductors, *Phys. Rev. B* **92**, 134501 (2015).

[108]A. Damask and G. Dienes, *Point Defects in Metals* (Gordon and Breach, 1963).

[109]M. Thompson, *Defects and Radiation Damage in Metals*, Cambridge Monographs on Physics (Cambridge University Press, 1974).

[110]M. Kirk and Y. Yan, Structure and properties of irradiation defects in  $\text{YBa}_2\text{Cu}_3\text{O}_{7-x}$ , *Micron* **30**, 507 (1999).

[111]J. Giapintzakis, W. C. Lee, J. P. Rice, D. M. Ginsberg, I. M. Robertson, R. Wheeler, M. A. Kirk, and M.-O. Ruault, Production and identification of flux-pinning defects by electron irradiation in  $\text{YBa}_2\text{Cu}_3\text{O}_{7-x}$  single crystals, *Phys. Rev. B* **45**, 10677 (1992).

[112]V. Sunko, P. H. McGuinness, C. S. Chang, E. Zhakina, S. Khim, C. E. Dreyer, M. Konczykowski, H. Borrman, P. J. W. Moll, M. König, D. A. Muller, and A. P. Mackenzie, Controlled Introduction of Defects to Delafossite Metals by Electron Irradiation, *Phys. Rev. X* **10**, 021018 (2020).

[113]J. Westerveld, D. L. Cascio, H. Bakker, B. Loopstra, and K. Goubitz, Atomic disorder and superconductivity in  $\text{Ca}_3\text{Rh}_4\text{Sn}_{13}$ , *Journal of Physics: Condensed Matter* **1**, 5689 (1989).

[114]A. M. Campbell, The response of pinned flux vortices to low-frequency fields, *J. Phys. C: Sol. Stat. Phys.* **2**, 1492 (1969).

[115]R. Willa, V. B. Geshkenbein, R. Prozorov, and G. Blatter, Campbell response in type-II superconductors under strong pinning conditions, *Phys. Rev. Lett.* **115**, 207001 (2015).

[116]C. P. Bean, Magnetization of Hard Superconductors, *Phys. Rev. Lett.* **8**, 250 (1962).

[117]C. P. Bean, Magnetization of High-Field Superconductors, *Rev. Mod. Phys.* **36**, 31 (1964).

[118]P. Prommapan, M. A. Tanatar, B. Lee, S. Khim, K. H. Kim, and R. Prozorov, Magnetic-field-dependent pinning potential in  $\text{LiFeAs}$  superconductor from its Campbell penetration depth, *Phys. Rev. B* **84**, 060509 (2011).

[119]H. Kim, N. H. Sung, B. K. Cho, M. A. Tanatar, and R. Prozorov, Magnetic penetration depth in single crystals of  $\text{SrPd}_2\text{Ge}_2$  superconductor, *Phys. Rev. B* **87**, 094515 (2013).

[120]H. Kim, M. A. Tanatar, H. Hodovanets, K. Wang, J. Paglione, and R. Prozorov, Campbell penetration depth in low carrier density superconductor  $\text{YPtBi}$ , *Phys. Rev. B* **104**, 014510 (2021).

[121]S. Ghimire, F. Gaggioli, K. R. Joshi, M. Konczykowski, R. Grasset, E. H. Krenkel, A. Datta, M. A. Tanatar, S. Chen, C. Petrovic, V. B. Geshkenbein, and R. Prozorov, Nonmonotonic relaxation of campbell penetration depth from creep-enhanced vortex pinning, arXiv:2403.14891 (2024).

[122]R. Prozorov, A. Tsameret, Y. Yeshurun, G. Koren, M. Konczykowski, and S. Bouffard, Frequency dependent irreversibility line and unidirectional magnetic anisotropy in thin  $\text{YBa}_2\text{Cu}_3\text{O}_{7-x}$  films irradiated with heavy ions, *Physica C* **235-240**, 3063 (1994).

[123]S. Kumar, C. V. Tomy, A. K. Grover, G. Balakrishnan, and D. M. Paul, Crossover from more to less ordered vortex state on field-cooling a weakly pinned crystal of  $\text{Ca}_3\text{Rh}_4\text{Sn}_{13}$ , *AIP Conf. Proc.* **1512**, 1202 (2013).

[124]E. Helfand and N. R. Werthamer, Temperature and Purity Dependence of the Superconducting Critical Field,  $H_{c2}$ . II, *Phys. Rev.* **147**, 288 (1966).

[125]V. G. Kogan and R. Prozorov, Critical fields of superconductors with magnetic impurities, *Phys. Rev. B* **106**, 054505 (2022).

[126]R. Prozorov and V. G. Kogan, Practically universal representation of the Helfand-Werthamer upper critical field for any transport scattering rate, arXiv:2407.15000 (2024).